ELLIPTICAL ACCRETION DISKS IN ACTIVE GALACTIC NUCLEI

MICHAEL ERACLEOUS AND MARIO LIVIO

Space Telescope Science Institute, 3700 San Martin Drive, Baltimore, MD 21218; e-mail: eracleous@stsci.edu, mlivio@stsci.edu

JULES P. HALPERN

Columbia Astrophysics Laboratory, Columbia University, 538 West 120th Street, New York, NY 10027;
e-mail:jules@carmen.phys.columbia.edu

AND

THAISA STORCHI-BERGMANN

Departamento de Astronomia, IF-UFRGS, CP-15051, CEP 91501-970, Porto Allegre, RS, Brasil; e-mail:thaisa@if1.ufrgs.br

ABSTRACT

We present a calculation of the profiles of emission lines originating in a relativistic, *eccentric* disk, and show examples of the resulting model profiles. Our calculations are motivated by the fact that in about one-quarter of the double-peaked emission lines observed in radio-loud active galactic nuclei (and in the mildly active nucleus of NGC 1097), the red peak is stronger than the blue peak, which is contrary to the prediction of relativistic, circular disk models. Using the eccentric disk model we fit some of the observed profiles that cannot be fitted with a circular disk model. We propose two possible scenarios for the formation of an eccentric disk in an active galactic nucleus: (*a*) tidal perturbation of the disk around a supermassive black hole by a smaller binary companion, and (*b*) formation of an elliptical disk from the debris resulting from the tidal disruption of a star by the central black hole. In the former case we show that the eccentricity can be long-lived because of the presence of the binary companion. In the latter case, although the inner parts of the disk may circularize quickly, we estimate that the outer parts will maintain their eccentricity for times much longer than the local viscous time. If any of the observed double-peaked emission lines do indeed arise in an eccentric disk, their profiles are likely to vary due to precession of the disk, thus providing a means of testing our proposed scenario. We estimate that for a black hole with a mass of order $10^6 \ M_\odot$, the precision period due to general relativistic advance of the pericenter can be as short as a decade. However, for a black hole with a mass of the order of $10^8 \ M_\odot$ the precession period is of the order of a few centuries, be it due to general relativistic effects or due to the tidal effects of a binary companion. We suggest that it may nevertheless be possible to detect profile variability on much shorter timescales by comparing the evolution of the line profile with detailed model predictions. We argue that line-profile variability may also be the most promising discriminant among competing models for the origin of asymmetric, double-peaked emission lines.

Subject headings: galaxies: nuclei — galaxies: active — line: profiles — accretion, accretion disks — black hole physics

1. INTRODUCTION AND MOTIVATION

In the present working scenario for the nature of active galactic nuclei (hereafter AGNs), the primary source of power in these systems is a supermassive black hole which is accreting matter from the host galaxy through an accretion disk. The hot, inner parts of the accretion disk are thought to be the source of the observed high-energy continuum radiation, which is also believed to be the driver of the observed emission lines. Although appealing from a theoretical perspective, and generally assumed, the presence of an accretion disk has met with fairly limited observational evidence (see, for example, the reviews by Kinney 1992, 1994; and Netzer 1992). Kinematic evidence, in the form of double-peaked emission lines, which are characteristic of a rotating disk, is quite scarce. Until recently, only a handful of broad-line radio galaxies were known to display these unusual double-peaked emission lines, namely 3C 390.3 (Oke 1987; Pérez et al. 1988), Arp 102B (Chen, Halpern, & Filippenko 1989, hereafter CHF; Chen & Halpern 1989, hereafter CH), and 3C 332 (Halpern 1990). The recent survey of over 90 moderate-redshift, radio-loud AGNs by Eracleous & Halpern (1994, hereafter EH) has uncovered several more examples of double-peaked emission lines. Their collection (which contains both new and previously known cases) includes 19 examples of radio-loud AGNs whose Hα line profiles have double peaks or twin shoulders. Of these, 10 (the "disklike emitters") can be fitted reasonably well with a simple model of a circular, relativistic, Keplerian disk (see CHF and CH). These 10 objects make up a reasonably homogeneous class based on additional properties which they possess, namely (*a*) Balmer lines which are on the average twice as broad as those of typical radio-loud AGNs, (*b*) an optical continuum whose starlight fraction is considerably larger than in typical radio-loud AGNs, and (*c*) large equivalent widths of low-ionization forbidden lines and large [O I]/[O III] ratios compared to the average radio-loud AGN. These properties can be understood in the context of the physical model proposed by CH for Arp 102B, in which the inner disk is a hot ion torus illuminating the outer disk and driving the broad-line emission.

Of the 19 radio-loud objects in the collection of double-peaked emitters of EH, five have Hα profiles in which *the red peak (or shoulder) is stronger than the blue peak*. This is contrary to the prediction of *homogeneous, circular* relativistic disk models for the line profiles (e.g., CHF and CH), which require

the blue peak to be always stronger than the red peak due to Doppler boosting. In addition to the examples in the collection of EH, recent observations of the "mildly" active nucleus of NGC 1097 by Storchi-Bergmann, Baldwin, & Wilson (1992, hereafter SBW) have revealed broad, double-peaked Balmer lines, which are also asymmetric in the opposite sense than what circular relativistic disk models would predict (namely the red peak is stronger than the blue peak). NGC 1097 is classified as a low-ionization nuclear emission-line region (LINER) (e.g., Phillips et al. 1984) whose nuclear spectrum showed only *narrow* emission lines until 1991. The most recent spectra of NGC 1097 around Hα prior to those of SBW were taken in 1983 (W. Zheng and W. C. Keel, private communication) and show only the narrow Hα/[N II] complex without any evidence of broad lines.[1] The transformation of NGC 1097, as captured by the spectra of SBW, raises the possibility that the appearance of broad Balmer lines has to be associated with a cataclysmic event which occurred in the nucleus.

Motivated by the sense of the asymmetry in this small group of Hα line profiles, we refine the simple, circular disk model of CHF and CH. In particular, we construct models of eccentric disks, which can produce (in principle at least) profiles with a stronger red peak. In § 2 we present our calculation of profiles of emission lines from an elliptical, relativistic accretion disk. We present examples of model profiles to show how they are affected by the choice of model parameters, and we also compare the model predictions with observations. In § 3 we consider two possible scenarios for the formation of an elliptical disk, and we address the question of the lifetime of such disks against circularization. In § 4 we discuss the implications of our findings and consider additional signatures of elliptical disks, such as variability of the profiles due to disk precession. We also discuss the possibility of using the variability to test competing models of the origin of double-peaked emission lines. Finally, in § 5 we summarize our results and present our conclusions.

2. PROFILES OF EMISSION LINES FROM A RELATIVISTIC ELLIPTICAL DISK

2.1. *General Scheme for Calculating Line Profiles*

We compute the profiles of emission lines from an elliptical (Keplerian) disk in the weak field approximation by following the spirit of the calculations performed by CHF and CH. Their calculations are generalized to strong fields by Chen & Eardley (1991). For the sake of completeness, we begin with an outline of the technique and in the sections that follow we apply it to the special case of particles in elliptical orbits. The geometry is depicted in Figure 1, which also serves as an illustration of the conventions used in the calculation. The Cartesian axes x', y', z' show the frame of the disk, chosen so that the disk lies in the (x', y')-plane. The observer's frame is indicated by the Cartesian axes x, y, z, with the observer along the positive z-axis at $z = +\infty$. The line of sight (z-axis) is inclined with respect to the rotation axis of the disk (z'-axis) by an angle i, as shown in Figure 1. The calculation is carried out in polar coordinates (r, θ, φ) and (r, θ', φ'), where the primed angles are measured in the frame of the disk. The plane of the disk corresponds to $\theta' = \pi/2$

[1] A spectrum taken in 1985 (Busko & Steiner 1990) also shows no evidence for a broad Hα line but the wavelength coverage is rather narrow and hence the presence of a broad Hα line in 1985 cannot be conclusively ruled out.
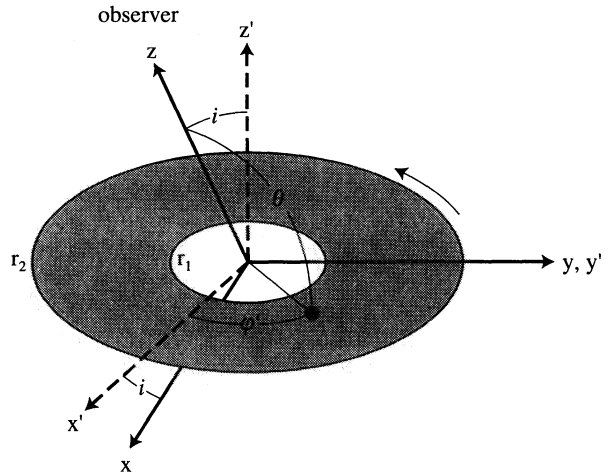

FIG. 1.—Geometry and coordinate systems used in the general scheme of profile calculations.

and φ' is the azimuthal coordinate around the disk. The angles are related via

$$\sin \varphi' = \sin \theta \sin \varphi , \tag{1}$$

$$\cos \theta = \sin i \cos \varphi' . \tag{2}$$

The central object is assumed to be a Schwarzschild black hole of mass M, located at the origin. Throughout this calculation we use units in which $G = c = 1$ (where G is the gravitational constant and c is the speed of light), and we adopt the gravitational radius as the unit of length. Hence we define the dimensionless radial coordinate $\xi \equiv r/r_g$, where $r_g \equiv GM/c^2 = M$ is the gravitational radius.

The total observed line flux from the disk is given by

$$F = \int dv \int\int d\Omega\, I_v , \tag{3}$$

where v, I_v, and $d\Omega$ are respectively the frequency, specific intensity (flux per unit frequency per unit solid angle) and solid angle element *as measured in the frame of the observer*. By using the invariance of the quantity I_v/v^3, the specific intensity can be transformed to the frame of the emitter (denoted by the subscript " e "). The solid angle $d\Omega$ is most conveniently expressed in terms of b, the impact parameter at infinity, as $d\Omega = b\, db\, d\varphi/d^2$, where d is the distance to the source. This expression allows one to deal with the difference caused by light bending between the solid angle in the frame of the disk and the solid angle in the frame of the observer. The expression for the total line flux then becomes

$$F = \frac{1}{d^2} \int dv \int\int b\, db\, d\varphi\, I_{v_e}\!\left(\frac{v}{v_e}\right)^3 , \tag{4}$$

where now v_e and I_{v_e} are the frequency and the specific intensity *as measured in the frame of the emitter*. The line profile itself is described by the function F_X, which is defined by $F = \int F_X\, dX$, where $1 + X = v/v_0$, and v_0 is the rest frequency of the line (X is effectively the redshift and F_X is the line flux per unit redshift interval). As noted by CH, in general $v_0 \neq v_e$ because the line can be locally broadened (e.g., due to turbulent

motions or electron scattering). From equation (4) and the definition of F_X it follows that

$$F_X = \frac{v_0}{d^2} \int\int b\, db\, d\varphi\, I_{v_e}\left(\frac{v}{v_e}\right)^3 .$$ (5)

The impact parameter can be expressed in the weak field approximation in terms of ξ, the dimensionless radial coordinate (CH), as

$$\frac{b}{r} \approx (1 - \sin^2 i \cos^2 \varphi')^{1/2}\left[1 + \frac{1}{\xi}\left(\frac{1 - \sin i \cos \varphi'}{1 + \sin i \cos \varphi'}\right)\right] ,$$ (6)

where the term proportional to ξ^{-1} is the first-order correction for light bending. Using equation (6), and expressing $d\varphi$ in terms of φ' with the help of equations (1) and (2), equation (5) becomes

$$F_X = \frac{M^2 v_0 \cos i}{d^2} \int\int \xi\, d\xi\, d\varphi'\, I_{v_e} D^3 \Psi(\xi, \varphi') ,$$ (7)

where $\Psi(\xi, \varphi')$ is given by

$$\Psi(\xi, \varphi') = 1 + \frac{1}{\xi}\left(\frac{1 - \sin i \cos \varphi'}{1 + \sin i \cos \varphi'}\right)$$ (8)

and $D \equiv v/v_e$ is the Doppler factor, which depends on the positions and velocities of the particles in the disk, as well as on the assumed metric. Assuming that the trajectories are known, so that the Doppler factor can be calculated, and that I_{v_e} is specified, equation (7) gives the profiles of the emergent emission lines. We note that equation (7) involves the *local* properties of the emitting region (the disk) and the *local* coordinate system, and gives the profiles of the emission lines *as seen in the frame of an observer at infinity*. Because we have used an approximate expression for b/r, equation (7) is valid only in the weak field approximation, which breaks down for $\xi \lesssim 100$ (as was also noted by Fabian et al. 1989). By adopting the emissivity law and Doppler factor of CH, equation (7) reduces to their expression for the line profile, where their function $g(D)$ is related to our $\Psi(\xi, \varphi')$ via $g(D) = 1/2[\Psi(\xi, \varphi') + \Psi(\xi, \pi - \varphi')]$.

2.2. *The Doppler Factor for Particles in an Elliptical Disk*

The Doppler factor can, in general, be computed by considering the four-velocity of the emitting particles. The four-momentum of a photon originating at radius r is $p^\alpha = hvP^\alpha$ where P^α is given by (CHF)

$$P^\alpha = \left\{\left(1 - \frac{2M}{r}\right)^{-1}, -\left[1 - \left(\frac{b}{r}\right)^2\left(1 - \frac{2M}{r}\right)\right]^{1/2}, -br^2, 0\right\} .$$ (9)

The energy of a photon in the rest frame of the emitter is $hv_e = p^\alpha u_\alpha = hvP^\alpha u_\alpha$, where u_α is the four-velocity of the emitting particle. Hence, from the definition of the Doppler factor it follows that $D \equiv v/v_e = 1/P^\alpha u_\alpha$. For a circular Keplerian disk, the explicit expression for the Doppler factor was derived by CHF and is given in their equation (4). Here we derive the corresponding expression for an elliptical Keplerian disk.

We assume that the elliptical disk is made up of nested elliptical annuli, which in principle need not have a constant eccentricity. The projected position of the observer in the plane of the disk is on the positive x'-axis, at $x' = +\infty$. Each annulus is described by its pericenter distance $\tilde\xi$ (in units of the gravitational radius), and its eccentricity e. It is assumed that all
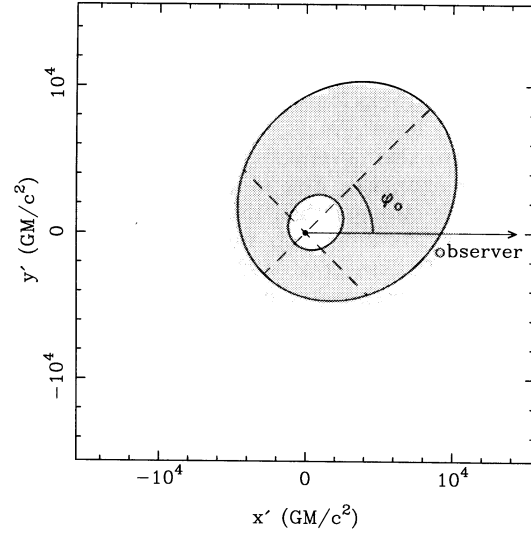

FIG. 2.—Top view of an elliptical disk, showing the definition of the orientation angle φ_o. The central massive object is located at the origin. In this illustrative example the disk has an eccentricity of 0.5 and its inner and outer boundaries have pericenter distances 1000 and 5000r_g, respectively.

annuli share a common major axis, which makes an angle φ_o with the x'-axis, as shown in Figure 2. The trajectory of a particle in a given annulus is described by

$$\xi(\varphi') = \frac{\tilde\xi(1 + e)}{1 - e\cos(\varphi' - \varphi_o)} .$$ (10)

In this convention, $\varphi_o = 0$ corresponds to the apocenter direction being coincident with the positive x'-axis, i.e., toward the observer. The line-emitting part of the disk is bound by inner and outer elliptical annuli of pericenter distances $\tilde\xi_1$ and $\tilde\xi_2$, respectively. The four-velocity of a particle in the disk at an azimuthal angle φ', on a trajectory of pericenter distance $\tilde\xi$, is

$$u_\alpha = \gamma\left[\left(1 - \frac{2}{\xi}\right)^{1/2}, \beta_r, \frac{r\beta_{\varphi'}\sin i \sin\varphi}{(1 - 2/\xi)^{1/2}}, \frac{r\beta_{\varphi'}\sin\theta(1 - \sin^2 i \sin^2\varphi)^{1/2}}{(1 - 2/\xi)^{1/2}}\right] ,$$ (11)

where ξ is given by equation (10) above, and β_r, $\beta_{\varphi'}$ and γ are defined by

$$\beta_r = \frac{e\sin(\varphi' - \varphi_o)}{[\tilde\xi(1 + e)]^{1/2}} ,$$ (12)

$$\beta_{\varphi'} = \frac{1 - e\cos(\varphi' - \varphi_o)}{[\tilde\xi(1 + e)]^{1/2}} ,$$ (13)

$$\gamma = (1 - u^i u_i)^{-1/2}, \quad i = r, \theta', \varphi' .$$ (14)

Substituting the expression for u_α in the general expression for D, replacing all trigonometric functions of φ and θ with functions of φ' with the help of equations (1) and (2), and rescaling the radial coordinate to dimensionless units, one obtains the following expression for the Doppler factor

$$\frac{1}{D} = \gamma\left\{\left(1 - \frac{2}{\xi}\right)^{-1/2} - \frac{[1 - (b/r)^2(1 - 2/\xi)]^{1/2}e\sin(\varphi' - \varphi_o)}{\xi^{1/2}(1 - 2/\xi)^{3/2}[1 - e\cos(\varphi' - \varphi_o)]^{1/2}} + \frac{(b/r)[1 - e\cos(\varphi' - \varphi_o)]^{1/2}\sin i \sin\varphi'}{\xi^{1/2}(1 - 2/\xi)^{1/2}(1 - \sin^2 i \cos^2\varphi')^{1/2}}\right\} ,$$ (15)

where b/r in the weak field approximation is given directly by equation (6), and γ can be evaluated from equation (14) to give

$$\gamma = \left\{ 1 - \frac{e^2 \sin^2 (\varphi' - \varphi_o) + (1 - 2/\xi)[1 - e \cos (\varphi' - \varphi_o)]^2}{\xi(1 - 2/\xi)^2[1 - e \cos (\varphi' - \varphi_o)]} \right\}^{-1/2}.$$

(16)

All the necessary ingredients for the calculation of line profiles are now available. The expression for D from equation (15) above can be substituted in equation (7) and the integral evaluated, with ξ and $d\xi$ taken from equation (10) and a suitable choice of the specific intensity. As a consistency check, we note that by setting $e = 0$ in our equations (the circular disk limit) we recover the results of CHF and CH. We note in conclusion that this calculation treats the case of an optically thick disk. The extension to an optically thin disk is straightforward, and is described in detail in CH, CHF, and Chen & Eardley (1991).

2.3. *Examples of Model Line Profiles and Comparison with Observations*

In order to explore the shapes of profiles produced by the elliptical disk model and to investigate how they are affected by changes in the model parameters, we have computed a series of model profiles for different combinations of parameters. We have adopted a prescription for the specific intensity of the line given by (see also CH)

$$I_{v_e} = \frac{1}{4\pi} \frac{\epsilon_o \, \xi^{-q}}{\sqrt{2\pi} \, \sigma} \exp \left[- \frac{(v_e^2 - v_o^2)}{2\sigma^2} \right],$$

(17)

where $\epsilon(\xi) = \epsilon_0 \xi^{-q}$ is the line emissivity. In this prescription, the local broadening is represented by a Gaussian profile in the frame of the emitter. The width of the local profile is determined by the broadening parameter σ, which can also be expressed in velocity units via $v_\sigma = c\sigma/v_o$. For the purpose of evaluating the integral in equation (7) one can use the definitions of X and D to write the specific intensity as

$$I_{v_e} = \frac{1}{4\pi} \frac{\epsilon_o \, \xi^{-q}}{\sqrt{2\pi} \, \sigma} \exp \left[- \frac{(1 + X - D)^2 v_o^2}{2D^2\sigma^2} \right].$$

(18)

The adopted line emissivity varies with *the radial distance from the central object*. This is a reasonable parameterization if, for example, the line emission from the disk is driven by illumination from a central extended source of ionizing radiation, in which case one would expect $\epsilon(\xi) \propto \xi^{-3}$. This prescription may also be plausible if the line emission is powered by energy dissipation in the disk, since in such a case the parts of the disk near pericenter may contribute more than the parts near apocenter. We note that in cataclysmic variable disks, where emission lines are thought to be powered by local dissipation, it is found observationally that the line emissivity varies as $\epsilon(\xi) \propto \xi^{-3/2}$ (Horne & Saar 1991). Alternative prescriptions may include an emissivity which is constant along a streamline and varies with the pericenter distance of an annulus, or an emissivity computed numerically from photoionization models (e.g., Dumont & Collin-Souffrin 1990). The effects of Keplerian shear on the optical depth in the lines (Horne & Marsh 1986) can, in principle, be included by introducing a non-axisymmetric disk emissivity.

The model has seven free parameters, namely the inner and outer pericenter distances of the line-emitting part of the disk

(ξ_1 and ξ_2), the inclination angle (i), the emissivity power-law index and the broadening parameter (q and σ), and the eccentricity and major axis orientation of the elliptical rings (e and φ_o). In practice, the profile shapes are not very sensitive to the broadening parameter, and the emissivity power-law index can be constrained by our theoretical prejudices. In the examples and fits that we present below the eccentricity was assumed to be constant and uniform throughout the disk. In Figure 3, we present sequences of model line profiles which show the effects of model parameters on profile shapes. Some of the more prominent characteristics of the line profiles are as follows.

1. The line profile splits into a double-peaked structure due to rotation. There is a net gravitational and transverse redshift of the entire line. The fractional gravitational shift is $(\Delta\lambda/\lambda)_{grav} \sim \xi_1^{-1}$, and the fractional transverse shift is $(\Delta\lambda/\lambda)_{trans} \sim (2\xi_1)^{-1}$, where ξ_1 is the inner pericenter distance (or inner radius) of the line-emitting part of the disk.

2. The relative sizes of the two peaks are determined by a competition between Doppler boosting, which always tends to enhance the blue peak, and the radial velocity field of the disk, which can boost either of the two peaks depending on the major axis orientation. Consequently, the blue peak is not necessarily higher than the red peak, as is the case for circular disk models. Furthermore, for suitable choices of the disk (major axis) orientation, the ratio of the blue peak to the red peak (the asymmetry) can be larger than what circular disks produce.

3. For the moderate eccentricities that we have focused on ($e \le 0.55$), and for power-law emissivity distributions that do not weigh the emissivity heavily toward the center of the disk, i.e., for power-law indices $q \lesssim 2.5$, the strongest of the two peaks is closest to the rest wavelength of the line. This is because the dominant contribution to the flux under the strongest peak comes from regions of the disk in the direction of apocenter, where the velocities of particles in the disk are low. If the emissivity is weighted heavily toward the inner parts of the disk, the dominant contribution to the flux under the strongest peak is due to the area of the disk near pericenter, where the particle velocities are high. It is thus possible to adjust the relative sizes of the two peaks by a suitable choice of the emissivity power-law index.

The eccentric disk model was used to try to fit those double-peaked Hα profiles from the collection of EH that cannot be reproduced by a circular disk model, and in addition the Hα profile of NGC 1097 (SBW); a total of 10 systems. The profiles fall under two general types: (*a*) those in which the red peak is stronger than the blue peak, which is contrary to the predictions of circular disk models, and (*b*) those in which the blue beak is stronger than the red peak but the particular combination of relative peak strengths and separation cannot be reproduced by circular disk models. The elliptical disk model successfully reproduces a large fraction of the observed profiles but there are, nevertheless, also cases in which it clearly fails. Table 1 provides a list of objects whose Hα profiles can be successfully fitted with an elliptical disk model, and includes six out of the 10 objects mentioned above. The fits themselves are shown in Figure 4. In the case of two objects (TEX 1156+21 and PKS 2300−18), the model can reproduce the wings and pronounced shoulders of the Hα profile but it leaves behind residual emission at low velocities. Although emission from material beyond the outer disk can be invoked to explain the residuals, it is difficult to assess whether a disk model provides an appropriate description of the line profile. Hence these two
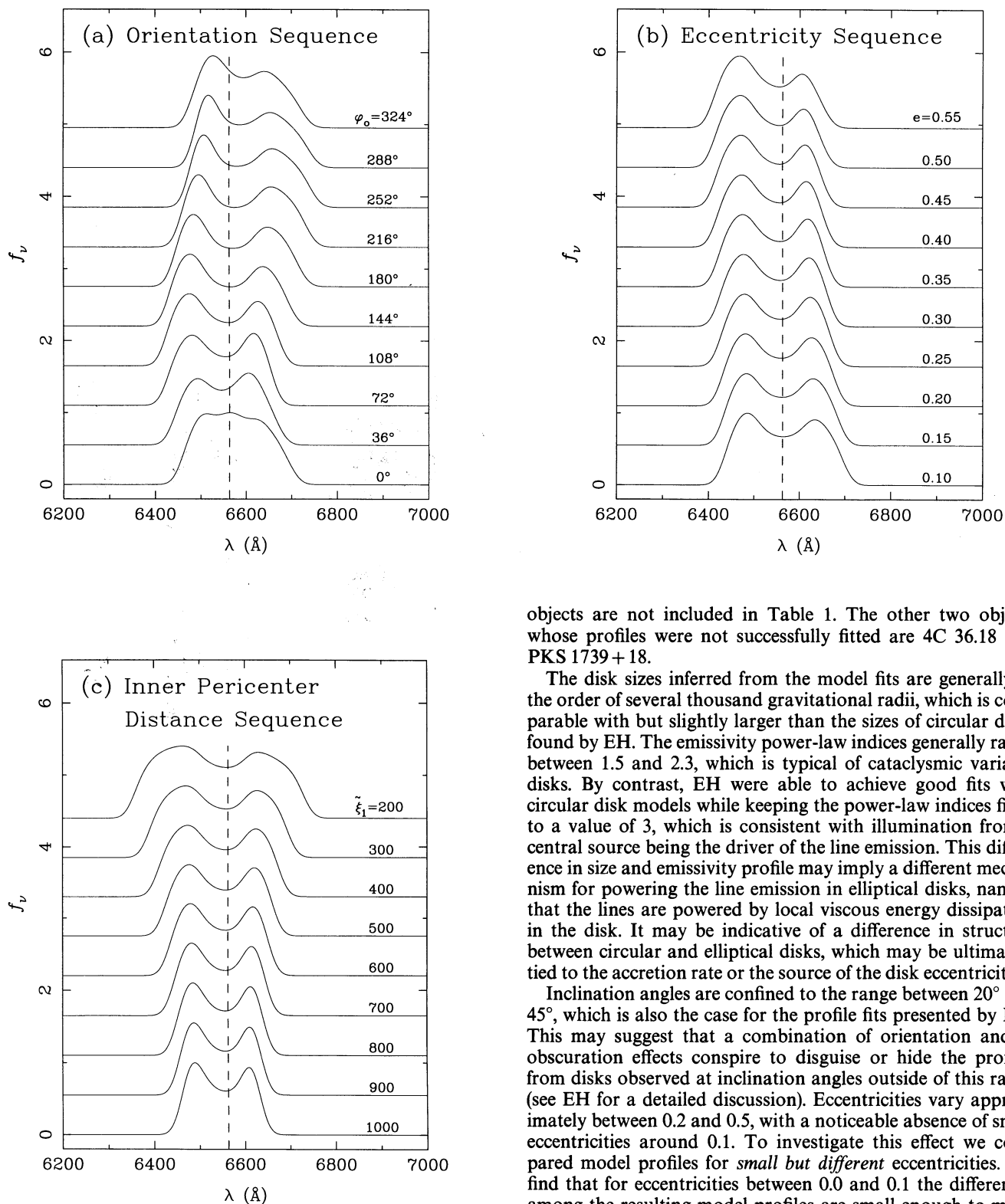
(a) Orientation Sequence

(b) Eccentricity Sequence

(c) Inner Pericenter Distance Sequence

FIG. 3.—Sequences of examples of model Hα profiles showing the effects of selected disk parameters on the profile shapes: (a) major axis orientation, (b) eccentricity, (c) inner pericenter distance. In each sequence only one parameter is varied, while all other are held constant to the following values: $\tilde{\xi}_1 = 500$, $\tilde{\xi}_2 = 2500$, $q = 3$, $i = 30°$, $\sigma = 800$ km s^{-1}, $e = 0.3$, $\varphi_o = 90°$. The dashed vertical line shows the rest wavelength of the line. All profiles have been arbitrarily normalized to unit maximum.

objects are not included in Table 1. The other two objects whose profiles were not successfully fitted are 4C 36.18 and PKS 1739 + 18.

The disk sizes inferred from the model fits are generally of the order of several thousand gravitational radii, which is comparable with but slightly larger than the sizes of circular disks found by EH. The emissivity power-law indices generally range between 1.5 and 2.3, which is typical of cataclysmic variable disks. By contrast, EH were able to achieve good fits with circular disk models while keeping the power-law indices fixed to a value of 3, which is consistent with illumination from a central source being the driver of the line emission. This difference in size and emissivity profile may imply a different mechanism for powering the line emission in elliptical disks, namely that the lines are powered by local viscous energy dissipation in the disk. It may be indicative of a difference in structure between circular and elliptical disks, which may be ultimately tied to the accretion rate or the source of the disk eccentricity.

Inclination angles are confined to the range between 20° and 45°, which is also the case for the profile fits presented by EH. This may suggest that a combination of orientation and/or obscuration effects conspire to disguise or hide the profiles from disks observed at inclination angles outside of this range (see EH for a detailed discussion). Eccentricities vary approximately between 0.2 and 0.5, with a noticeable absence of small eccentricities around 0.1. To investigate this effect we compared model profiles for *small but different* eccentricities. We find that for eccentricities between 0.0 and 0.1 the differences among the resulting model profiles are small enough to make them indistinguishable in view of the available data. This, however, may depend on the other model parameters as well, most notably the orientation of the major axis relative to the line of sight. This uncertainty in determining the eccentricity suggests the possibility that some of the line profiles fitted with circular disk models by EH may be slightly eccentric.
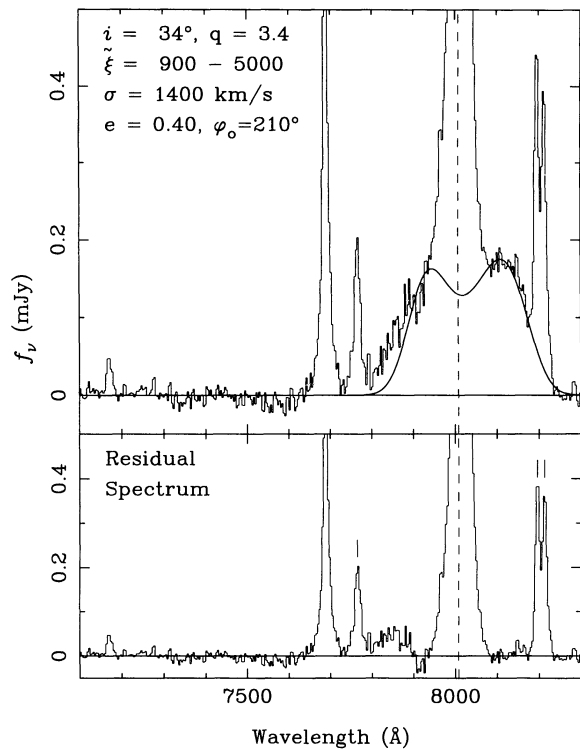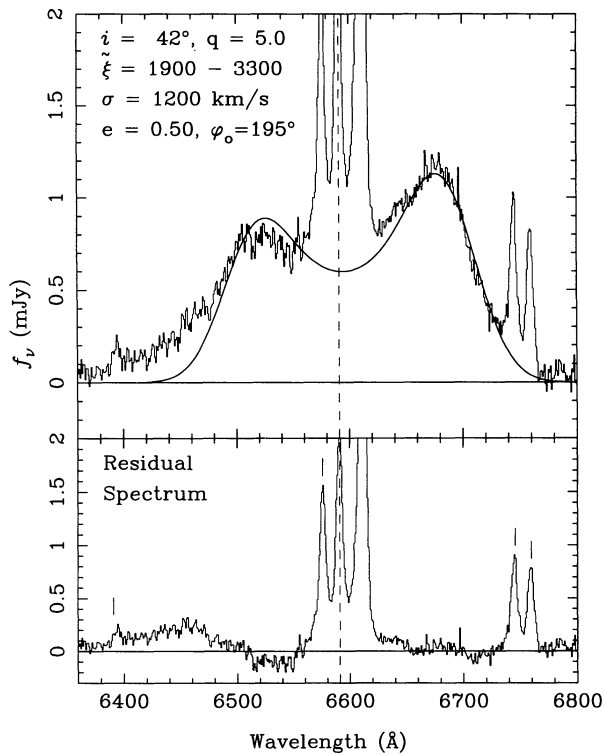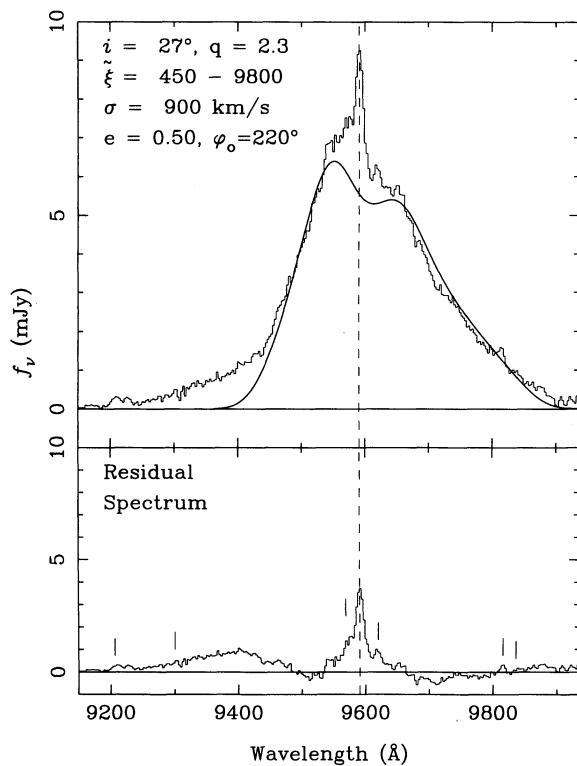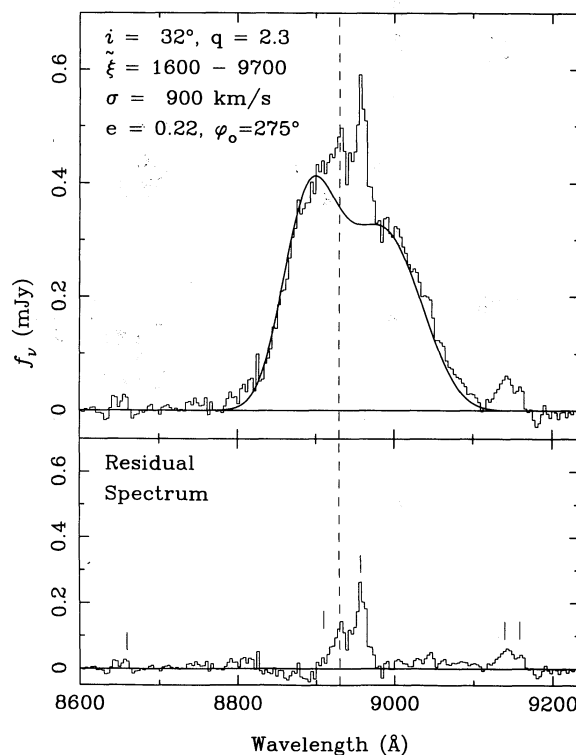
FIG. 4a

FIG. 4b

FIG. 4c

FIG. 4d

FIG. 4.—Reasonably good fits to observed Hα profiles using the elliptical disk model. (a) 3C 17, (b) NGC 1097, (c) B2 0742+31, (d) PKS 0857−19, (e) PKS 1020−103, (f) 3C 382. The model parameters are the inner and outer pericenter distances of the line-emitting part of the disk ($\tilde{\xi}_1$ and $\tilde{\xi}_2$), the inclination angle (i), the emissivity power-law index and the broadening parameter (q and σ), and the eccentricity and major axis orientation of the elliptical rings (e and φ_o). In each figure the upper panel shows the observed Hα profile after subtraction of the underlying continuum, along with the model fit (*thick solid line*). The lower panel shows the residual spectrum after subtraction of the fit. The dashed vertical line marks the wavelength of the narrow Hα line. The markers in the lower panel show the expected positions of the narrow forbidden lines, namely: [O I] λ6300 and λ6363, [N II] λ6548 and λ6583, and [S II] λ6716 and λ6731.
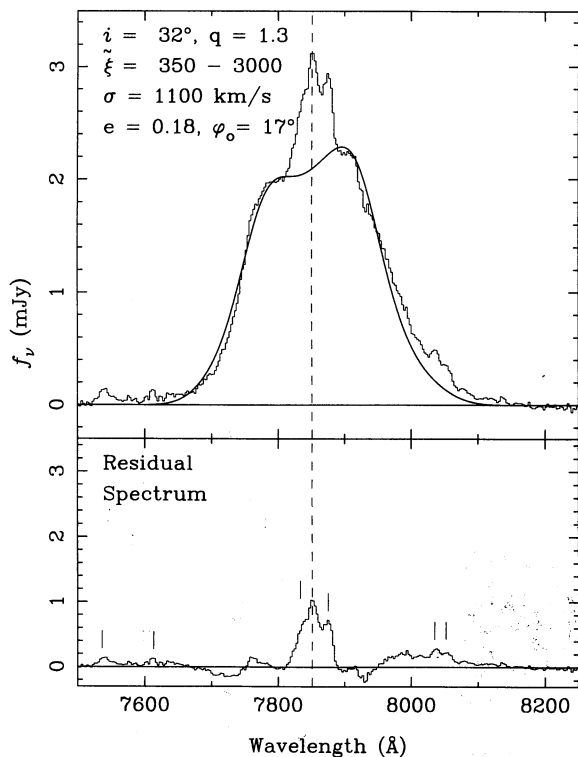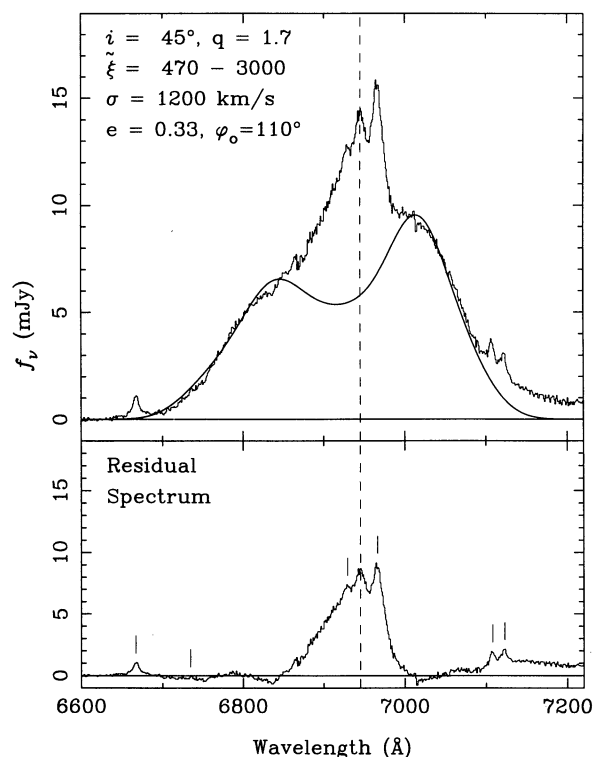
Fig. 4e

Fig. 4f

The results for NGC 1097 stand out because the fitted characteristics of its hypothesized disk are quite different from those of the radio-loud AGNs that make up the remainder of the list in Table 1. In particular, the line-emitting region in NGC 1097 resembles an eccentric ring rather than a disk, with a width smaller than its radius. Although the emissivity appears to fall steeply with radius, the line-emitting ring is so narrow that the emissivity drops only by an order of magnitude from its inner to its outer edge. This may be a consequence of the disk formation mechanism, which we discuss in detail in the sections that follow.

3. FORMATION OF ELLIPTICAL DISKS

The idea of elliptical accretion disks is by no means a new one, as it has already been invoked to explain phenomena observed in stellar accretion-powered systems. In particular,

the standard interpretation of the "superhump" phenomenon in dwarf novae involves the formation of an elliptical disk around the white dwarf primary via a tidally induced eccentric instability (Vogt 1982; Warner 1985; Whitehurst 1988; Osaki 1989; Lubow 1991a, b, 1992). Compelling evidence in support of this view comes from the recent study of the ultrashort period binary AM CVn by Patterson, Halpern, & Shambrook (1993), who find that the twin troughs of the numerous helium absorption lines alternate in depth periodically, suggesting that they originate in a precessing elliptical disk. In a cataclysmic binary the companion star is a natural source of the perturbations responsible for the eccentricity and precession of the disk. In an active nucleus, by contrast, there is no obvious perturber, but this does not preclude the possible existence of an elliptical accretion disk. In the sections that follow, we suggest two possible scenarios for the formation of elliptical

TABLE 1

FIT PARAMETERS FOR OBSERVED PROFILES[a]

Object	z	Asymmetry[b]	i (± 2)	q (± 0.3)	$\tilde{\xi}_1$ (± 100)	$\tilde{\xi}_2$ (± 500)	σ (km s^{-1}) (± 300)	e (± 0.10)	φ_o (± 10)
3C 17	0.220	$R > B$	34°	3.4	900	5000	1400	0.40	210°
NGC 1097	0.005	$R > B$	42	5.0	1900	3300	1200	0.50	195
B2 0742+31	0.462	$B > R$	27	2.0	450	9800	900	0.50	220
PKS 0857−19	0.360	$B > R$	32	2.3	1600	9700	900	0.22	275
PKS 1020−103	0.197	$R > B$	32	1.3	350	3000	1100	0.18	17
3C 382	0.059	$R > B$	45	1.7	470	3000	1200	0.33	110

[a] The quantity in parentheses accompanying each model parameter label shows the approximate uncertainty in the determination of that parameter in the model fit. These were obtained by perturbing the model parameters about their best values until an acceptable fit was no longer possible.

[b] $R > B$ indicates that the profile asymmetry is such that the red peak (or shoulder) is stronger than the blue one, while $B > R$ indicates the opposite asymmetry.

disks in AGNs. The first one is analogous to the mechanism invoked in cataclysmic binaries, namely that the disk becomes eccentric due to the presence of a binary companion to the accreting black hole. The second scenario, which is inspired by the sudden appearance of the double-peaked Balmer lines in NGC 1097 (see § 1), is one in which the elliptical disk is formed by the debris released from the disruption of a star by a supermassive black hole in the active nucleus.

3.1. *Elliptical Disks due to Binary Black Holes*

The formation of massive black hole binaries in AGNs was first proposed by Begelman, Blandford, & Rees (1980), who also investigated their evolution. In their scenario, the supermassive binary forms as a result of the merger of two parent galaxies, each with its own nuclear black hole. The scenario is thus particularly applicable to the most common hosts of radio-loud AGNs, namely elliptical galaxies, which are likely to be the products of mergers. For conditions typical of the cores of giant ellipticals, the two black holes encounter each other and form a bound system in a relatively short time, of order 10^6 yr. The binary system spends most of its life as a "hard" binary, one in which the orbital velocities are *at least* as large as the stellar velocity dispersion in the core (typically a few hundred km s^{-1}). The lifetime of the hard binary can vary between 10^8 and 10^{10} yr, depending on how efficiently energy is removed by encounters with stars. During this stage, the evolution of the binary may also be affected by the accretion of gas from the host galaxy on to the more massive of the two black holes (hereafter the primary). Accretion of gas will cause the orbit to contract on a timescale $\tau_{gas} \sim 10^8 \, M_8 \, (\dot{M}/1 \, M_\odot$ yr$^{-1})^{-1}$ yr, where M_8 is the mass of the primary in units of 10^8 $M_\odot$. When the orbital separation shrinks to about 0.01 pc gravitational radiation becomes the dominant energy loss mechanism and the binary is driven to coalescence on a timescale of $\tau_{coal} \sim 3 \times 10^5 \, q^2 (1 + q)^{-1} \, M_8^{-3} \, a_{16}^4$ yr, where q is the mass ratio ($q \equiv M/m$, where m is the mass of the less massive black hole), and a_{16} is the orbital separation in units of 10^{16} cm.

In the hard binary phase, in which the supermassive binary is most likely to be found, the orbital separation is of order 0.1–1 pc (10^{17}–10^{18} cm), and the corresponding orbital period is

$$P_{orb} \approx 54 \left(\frac{q}{1+q} \right)^{1/2} a_{17}^{3/2} M_8^{-1/2} \text{ yr} , \qquad (19)$$

where a_{17} is the orbital separation in units of 10^{17} cm. One would expect the tidal effects of the secondary black hole on an accretion disk around the primary to be analogous to the effects of the tidal field of the secondary star in a cataclysmic variable on the accretion disk around the white dwarf. These effects have been studied in great detail by several authors [e.g., Lubow 1991a, b, 1992; Hirose & Osaki 1990; Whitehurst 1988, 1994] in the context of the superhump phenomenon observed in cataclysmic binaries. It is generally found that for extreme mass ratios, $q \geq 4$, the disk is unstable to tidal perturbations, with the result that eccentricity can be generated at the 3:1 resonance. We suggest, by analogy, that the same instability will operate in supermassive black hole binaries, causing the accretion disk around the primary black hole to develop an eccentricity (in response to the tidal field of the secondary). The timescale for the growth of the eccentricity can be estimated using the results of Lubow (1991a) as $\tau_{ecc} \sim q^2 \, P_{orb}$, which

gives about 5400 yr for the parameter values in equation (19) (taking $q \sim 10$). Since this is much shorter than the expected lifetime of the hard binary, one would expect that the disk will become eccentric very quickly and maintain its eccentricity for periods much longer than the growth time. An additional consequence of the short growth time is that the *entire* disk will quickly respond to the tidal field and the eccentricity will be uniform and constant throughout the disk. This justifies a posteriori the assumption of a uniform, constant eccentricity disk made in § 2.3. Because the source of the tidal field is long lived, the eccentric disk may also be long lived and it should manifest itself through the profiles of emission lines that it emits. Precession of the eccentric disk may have additional observational consequences, which we will discuss further in § 4.

In our fits to the line profiles presented in § 2.3 we have not included any wavelength shifts of the entire line, other than what is required by the disk model. In the context of the binary black hole scenario, we make the implicit assumption that the black hole surrounded by the accretion disk has a negligible orbital velocity, i.e., that it is considerably more massive than its companion ($q \gg 1$). The orbital velocity of the primary in a supermassive binary is $v_1 \lesssim 800 a_{17}^{-1/2} \, M_8^{1/2}$ km s^{-1} (for $q \geq 4$, the smallest mass ratio for which the eccentric instability can be excited). This will be further reduced by projection along the line of sight to the observer. For the range of inclination angles in Table 1, the wavelength shift one can expect due to the orbital motion of the accreting black hole is $\Delta\lambda < 12$ Å, which is very difficult, and perhaps impossible, to discern in view of the uncertainties in the best-fit model parameters.

3.2. *Elliptical Disks due to Tidal Disruption of Stars by Supermassive Black Holes*

Our second scenario for the formation of elliptical disks is inspired by the sudden appearance of double-peaked Balmer lines in the LINER–like nucleus of NGC 1097. We suggest that a transient accretion disk may form as a result of the capture and disruption of a passing star by a supermassive black hole in an AGN. The mechanism and outcome of tidal disruption events has been studied in detail in the context of fueling the nuclear activity (see reviews by Rees 1988, 1990). On a close passage near a supermassive black hole, a star is disrupted if the tidal acceleration across it at pericenter exceeds its surface gravity. This implies the presence of a tidal disruption radius, r_T, around the black hole, within which stars of a given mass will be disrupted. This radius can be expressed in units of the gravitational radius as $\xi_T \equiv r_T/r_g = 34 \, r_* \, m_*^{-1/3} \, M_6^{-2/3}$, where r_* and m_* are respectively the radius and mass of the star in solar units, and M_6 is the mass of the black hole in units of 10^6 $M_\odot$. One generally distinguishes between two types of tidal encounters (cf. Press & Teukolsky 1977): weak encounters, during which the pericenter distance (in units of r_g) $\tilde{\xi}$ is of the same order as ξ_T, and strong encounters, in which $\tilde{\xi} \ll \xi_T$. We note that if $M > 10^8 \, M_\odot$ then $\xi_T < 2$, i.e., the tidal disruption radius for a 1 $M_\odot$ star is smaller than the Schwarzschild radius, and hence the star is swallowed whole without being disrupted.

The evolution of the post-disruption debris depends on the strength of the tidal encounter. We concentrate on the case of a weak encounter of a 1 $M_\odot$ star with a 10^6 $M_\odot$ black hole which has been much better studied and hence results are available for us to draw on. In this case, the postdisruption debris is uniformly distributed in energy and about one-half of it is bound to the black hole, while the other half escapes (Rees 1988; Evans & Kochanek 1989). The issue most relevant to

(and indeed crucial for) our purposes is the subsequent viscous evolution of the stream of bound, postdisruption debris. Since the orbits of this debris are very eccentric, it is a very promising candidate for the formation of an elliptical accretion disk. This issue was addressed by Syer & Clarke (1992, 1993), who studied the evolution of the stream of postdisruption debris. Their numerical calculation, which begins with a stream of material qualitatively similar to that resulting from the disruption of a 1 $M_\odot$ star, shows that within a viscous time the debris forms a well-defined, eccentric disk. By scaling the relevant parameters appropriately, the viscous time may be expressed as (Frank, King, & Raine 1992, p. 99)

$$\tau_{\rm visc} \sim 56\alpha^{-4/5}\dot{m}^{-3/10}M_6^{3/2}\xi_3^{5/4} \text{ yr}, \qquad (20)$$

where $\dot{m}$ is the accretion rate in $M_\odot$ yr^{-1}, ξ_3 is the radius from the central object in units of $10^3 r_g$, and α is the viscosity parameter in the prescription of Shakura & Sunyaev (1973). The particle trajectories in the inner parts of the disk (within about 100 Schwarzschild radii, i.e., $\xi \lesssim 200$) are circular, due to the differential precession of the orbits very close to the black hole. This precession brings adjacent elliptical rings into oblique impact with each other and leads to rapid dissipation of energy and angular momentum through oblique shocks, and hence to rapid circularization (see discussion by Rees 1988, 1990; and also Cannizzo, Lee, & Goodman 1990). The general, analytical results of Syer & Clarke (1992, 1993) are applicable to the long-term evolution of the eccentric, outer disk, which is not strongly affected by relativistic differential precession. These results suggest that an elliptical disk will retain its eccentricity over a time which is at least as long as the viscous time (and even become more eccentric) rather than tend to circularize. The growth time for the eccentricity is much longer than the orbital timescale, which implies that the disk can be regarded as a quasi-equilibrium structure, consisting of nested elliptical orbits. The eccentricity need not necessarily be uniform and constant throughout the disk in this particular scenario, but instead it can increase smoothly with radius (Syer & Clarke 1992; Hirose & Osaki 1992). To assess the importance of this effect in fitting the Hα line profile of NGC 1097, we compared the line profile produced by an elliptical ring of constant eccentricity with that produced by a ring of smoothly varying eccentricity. The difference was found to be negligible because the elliptical ring in NGC 1097 is so narrow that the difference in eccentricity between its inner and outer part is small.

An issue that deserves further attention is the circularization of the disk due to general relativistic differential precession of elliptical rings (advance of the pericenter). One can make a rough estimate of the timescale for circularization up to a pericenter distance $\tilde{\xi}$ due to differential precession, by estimating the time it would take a ring at this pericenter distance to gain one full revolution over an adjacent ring of pericenter distance $\tilde{\xi} + \delta\tilde{\xi}$. If we take the width of a ring to be comparable to the local thickness of the disk, i.e., $\delta\tilde{\xi} \sim c_s/(\Omega r_g)$ (where c_s and Ω are the local sound speed and angular speed, respectively), we find that

$$\tau_{\rm circ} \sim 2 \times 10^4 \, M_6 \, T_5^{-1/2}(1+e)\tilde{\xi}_3^2 \text{ yr}, \qquad (21)$$

where T_5 is the local temperature in units of 10^5 K. Because of the circularization condition that we have adopted, this estimate should be regarded more as an upper limit to the circularization time. However, we expect the actual circularization time to differ from this limit only by a factor of a few. If this

estimate is taken at face value, it implies that the inner parts of the disk (up to $\tilde{\xi} \sim 100$) will circularize within a few years, which is comparable to the local viscous time. This is in agreement with the numerical results of Syer & Clarke (1992) and supports the plausibility of this rough estimate. The importance of differential precession in the evolution of the disk can be assessed by comparing the circularization time with the viscous time. The ratio of the two timescales is

$$\frac{\tau_{\rm visc}}{\tau_{\rm circ}} \sim 3 \times 10^{-3}\alpha^{-4/5}\dot{m}^{-3/10}M_6^{1/2}T_5^{1/2}(1+e)^{-1}\tilde{\xi}_3^{-3/4}. \qquad (22)$$

For $\tilde{\xi} \sim 100$ the two timescales are comparable and hence differential precession plays an important role in the evolution of the disk, which leads to a rapid circularization of its inner parts. For $\tilde{\xi} \gtrsim 1000$ the two timescales differ considerably, with $\tau_{\rm circ} \gg \tau_{\rm visc}$, which implies that differential precession will not have serious effects on the evolution of the *outer* disk, which is our proposed line-production site.

This scenario is particularly attractive for the case of NGC 1097, where the double-peaked Balmer lines appeared abruptly. The fact that the nucleus of NGC 1097 is only "mildly" active may imply a relatively small black hole ($M \sim 10^6 M_\odot$), which can readily disrupt stars before accreting them. The fact that the line-emitting region in NGC 1097 resembles a narrow ring lends further support to the tidal disruption hypothesis and suggests the possibility that the line emission may originate in the stream of postdisruption debris (e.g., Roos 1992; Kochanek 1994). The unbound debris which is moving quasi-radially away from the black hole is also a potential source of line emission at low velocities, but we find no evidence for such emission in the Hα profile of NGC 1097. In the context of this scenario one also expects the lifetime of the disk to be of the order of the viscous time, which is much shorter than the mean time between tidal disruption events ($\sim 10^4$ yr—Rees 1988, 1990) and the lifetime of the AGN, which may explain why the formation elliptical disks due to tidal disruption of stars, and spectral transformations like that of NGC 1097, are quite rare. Furthermore one would also expect the structure and properties of the elliptical ring to change rapidly (on a timescale comparable to the viscous time) as material from the ring is accreted, and hence the broad Hα profile to vary.

4. DISCUSSION

4.1. *Alternatives to Accretion Disk Emission, and Emission from Inhomogeneous Disks*

Emission from an accretion disk is not by any means the only possible origin of double-peaked emission lines. The most promising alternatives proposed so far are emission from a binary broad-line region (BLR) associated with a system of binary black holes and emission from the two-sided jets. Both of these scenarios are flexible enough to allow for a wide range of intensity ratios of the two peaks in a double-peaked profile, and they do not necessarily require the blue peak to be stronger than the red peak: the binary BLR scenario does not require specific strengths or displacements of the broad peaks, while the double-jet scenario relies on an arbitrary relation between the intensities of the two jets.

The former scenario was suggested by Gaskell (1983) to explain emission-line profiles whose broad emission peaks are displaced from the systemic velocity (e.g., 3C 227 and Mrk

668). The supermassive black hole binary invoked in this scenario is the same as the one we have described in § 3.1, with the difference that one (or both) of the black holes has a "classical BLR" associated with it, i.e., a system of clouds in bound orbits. The orbiting clouds are photoionized by radiation from the vicinity of the black hole and are the source of the broad emission lines. Each BLR produces its own single-peaked line, and the displacement of the broad peaks with respect to the systemic velocity is a result of the orbital motion of the binary. The latter scenario, which involves emission from a double-sided jet, or more generally material flowing radially along double cones, was suggested by Zheng, Binette, & Sulentic (1990) and applied to the variable, double-peaked Hα profile of 3C 390.3 by Zheng, Veilleux, & Grandi (1991). This model can fit the observed double-peaked line profiles, but it would probably require the cone opening angles to be rather large (about 30°–60°; see the application to 3C 390.3 by Zheng et al. 1991); otherwise it would tend to produce a pair of detached broad peaks. This suggests that the line emission is unlikely to originate in the jets that power the radio lobes, because these are thought to be highly collimated (see, for example, Sparks, Biretta, & Machetto 1994). If the jet scenario is to succeed, it is more likely that the line emission is the result of the interaction of the jet with the interstellar medium of the host galaxy (cf. Norman & Miley 1984; and also Wilson 1993, and references therein). This idea is also consistent with the observed width of the emission lines, which corresponds to velocities significantly lower than those thought to be typical of radio jets. The model can fit double-peaked profiles regardless of the relative sizes of the two peaks, but it produces the asymmetries by an ad hoc adjustment of the relative intensities of the two emitting cones. The understanding of jets is, at present, rather poor, and hence there are few detailed models available for comparison with observations. It may, nevertheless, be possible to use spectropolarimetric observations to constrain the geometry of the emitting region, thereby testing the applicability of jet scenarios.

In addition to the alternative scenarios which do not involve emission from an accretion disk, one can also envisage models of warped or inhomogeneous disks that can produce asymmetric emission-line profiles. A warped disk may form as a consequence of the Bardeen—Peterson effect (Bardeen & Peterson 1975), namely, a disk around a Kerr black hole, which at large distances is not in the equatorial plane of the hole, will twist so as to join smoothly with the equatorial plane, very close to the hole (i.e., within a distance of 10^2–10^4 r_g). Due to projection effects, parts of the disk moving toward and away from the observer will present different areas to the observer, thus producing asymmetric line profiles. The outer parts of the disk will precess due to the Lens–Thirring effect, causing the line profiles to vary in time. Inhomogeneities in the disk may take the form of spiral waves (e.g., Bunk, Livio, & Verbunt 1990; Chakrabarti & Wiita 1993a, 1994), or hot spots due to collisions or tidal encounters of the disk with passing stars or supermassive objects (e.g., Syer, Clarke, & Rees 1991; Kim & Yee 1992; Chakrabarti & Wiita 1993b). In both of these cases the inhomogeneities will boost the emissivity of the disk at selected velocities, thus producing asymmetries in the line profiles.

Since models for the origin of (asymmetric) double-peaked emission lines abound while data are rather scarce, distinguishing among models on the basis of snapshots of line profiles is a particularly challenging task. The key to constraining such models is probably the variability of the line profiles. Different models predict different patterns of variability, and some of the predictions are quite specific. Hence observations of variable line profiles can be used to test the above scenarios, as we discuss in more detail in the next section.

4.2. Precession of an Elliptical Disk, and Variability of Emission-Line Profiles

Because elliptical orbits in a Schwarzschild potential are not closed, their pericenter will advance with every revolution and hence cause the elliptical disk to precess. The precession per revolution of an orbit of pericenter distance ξ and eccentricity e is $\Delta\varphi = 6\pi\xi^{-1}(1 + e)^{-1}$ (e.g., Weinberg 1972), which implies a precession period of

$$P_{GR} \sim 10 \, M_6 \, \xi_3^{5/2} \text{ yr} \,. \tag{23}$$

This expression is not directly applicable to a large elliptical disk because the ratio of the outer to inner pericenter distances can be as large as 20 (see Table 1). Hence the inner part of the disk can circularize due to differential precession before the outer part precesses by a significant amount. Equation (23) can, nevertheless, be applied to a narrow elliptical ring, such as the hypothesized line-emitting ring of NGC 1097, where the inner and outer pericenter distances differ by less than a factor of 2.

An accretion disk around the primary in a supermassive binary black hole will also precess due to the direct tidal effects of the secondary. The precession period can be estimated using the results of Lubow (1992) as

$$P_{tidal} \sim 500\left(\frac{q_4^3}{1 + q_4}\right)a_{17}^{3/2}M_8^{-1/2} \text{ yr} \,, \tag{24}$$

where q_4 is the mass ratio in units of 4, the smallest mass ratio for which the eccentric instability can be excited in the disk. Hence in either one of our proposed scenarios for the formation of an elliptical disk we expect the emission lines originating in the disk to vary because of disk precession. The pattern of variability, i.e., the progressive changes in the line profile predicted by the precessing disk model, is depicted in Figure 3a, which presents a sequence of model profiles for different orientations of the major axis of the disk relative to the line of sight. As Figure 3a shows, the general character of the profile does not change considerably with the orientation of the disk, but the width of the line and the separation of the two peaks vary by almost a factor of 2. The relative sizes of the two peaks also vary considerably, with the blue peak being stronger than the red peak at some phases and weaker at others. We note that the precession period ultimately depends on the mass of the black hole (or the binary system parameters, in the case of a binary). In a binary black hole, both tidal and general relativistic effects contribute to the precession of the disk, with tidal effects dominating for primary black hole masses greater than $10^8 \, M_\odot$. The rather long precession period of the disk in a supermassive binary makes it impossible to observe this type of profile variability, but it does, however, provide a means of testing the scenario. If variability is observed, it can be used to constrain the masses of the two black holes, possibly to the extent of making this model untenable. General relativistic precession of an elliptical disk around a $10^6 \, M_\odot$ black hole is more likely to be observable because it would occur on a timescale of about a decade or less.

Profile variability also affords us a way of testing two of the alternative scenarios for asymmetric, double-peaked emission

lines, namely the binary BLR scenario and the inhomogeneous circular disk models. In particular, if the double-peaked emission lines are due to a binary BLR, the orbital motion of the binary should cause periodic shifts of the broad displaced peaks on a timescale equal to the orbital period. As argued by Gaskell (1983), the orbital periods of supermassive binaries with masses of the order of $10^9 M_\odot$ (as one would expect to find in luminous quasars) are of the order of centuries, which makes the observation of profile variability in existing data sets rather unlikely. If, however, the mass of the binary is of the order $10^8 M_\odot$ (as one expects to find in moderate-luminosity AGNs such as Seyfert and radio galaxies), the orbital period would be of the order of a few decades, as shown by equation (19), and hence shifts of the broad, displaced peaks would be more readily observable. This test has been applied to two of the double-peaked emitters, Arp 102B and 3C 332, by Halpern & Filippenko (1988, 1992). They find no discernible shifts in the peak positions in spectra spanning a period of about a decade, which allows them to place lower limits on the masses of the hypothesized supermassive binaries. The limits are $4 \times 10^9 M_\odot$ for Arp 102 B and $2 \times 10^{10} M_\odot$ for 3C 332, which are rather restrictive and tend to make the binary BLR hypothesis unlikely for these particular objects.

If, on the other hand, the double-peaked Balmer lines originate in a circular disk with local inhomogeneities (hot spots), we would expect the inhomogeneities to dissipate due to Keplerian shear on a timescale of order $\tau_{shear} \approx 2 r P_{Kep}/3h$, where $P_{Kep} = 0.03 M_6 \xi_3^{3/2}$ yr is the Keplerian period, r is the orbital radius, and h is the radial extent of the inhomogeneity. If we assume that the radial extent of an inhomogeneity is comparable to the local scale height of the disk we may express the dissipation timescale of inhomogeneities as

$$\tau_{shear} \sim 0.7 M_6 \xi_3 T_5^{-1/2} \text{ yr}, \tag{25}$$

which is exactly the same as the estimate made by Veilleux & Zheng (1991) by considering the sound crossing time of the disk. Thus, the dissipation time for disk inhomogeneities can vary between several months and a few decades, depending on the mass of the central black hole. The evolution of the line profiles can be modeled using the approach of CHF and CH with a disk emissivity that allows for small regions of enhanced emission, which are progressively smeared out with time in the azimuthal direction.

The effect of spiral waves on the line profiles from a circular disk has been modeled by Chakrabarti & Wiita (1993a, 1994). The resulting profiles can have the blue peak stronger than the red peak or vice versa, depending on the orientation of the spiral pattern and on the number of spiral arms. As the pattern precesses it causes profiles to vary with the possibility of the two peaks alternating in strength. Chakrabarti & Wiita (1994) have used this model to produce fits to the Hα profiles of Arp 102 B, and 3C 390.3 at two different epochs, which suggest a pattern rotation period of the order of a few decades, although changes in the profile can be detected in time intervals of a few years. They have also computed sequences of model profiles as a function of rotation phase of the spiral pattern, which in principle can be used for comparison with observations. The model profiles comprise multiple peaks or shoulders which shift in wavelength and change significantly in strength as the pattern rotates, a behavior that can be used to test the model. What appears to be rather uncertain at this point is whether coherent spiral waves can indeed persist over a large radial extent in accretion disks (see, e.g., Livio 1992 for a review).

Although *two-dimensional* simulations of accretion disks show coherent spiral patterns when the disks are characterized by relatively low Mach numbers (e.g., Savonije, Papaloizou, & Lin 1994), the patterns do not extend to the inner parts for high Mach numbers, nor do they appear well organized when the simulations are extended to three dimensions. In addition, the two-dimensional simulations of AGN disks tidally perturbed by a passing object by Chakrabarti & Wiita (1993b) show that the spiral patterns are often fragmented and not well organized. For the case of AGN disks, typical Mach numbers are of order 50; thus spiral waves are not expected to be the dominant angular momentum transport mechanism (e.g., Savonije et al. 1994). If viscosity exists, it tends to smear out the spiral pattern. On the positive side, Savonije et al. (1994) also find that even though spiral waves in cool, high Mach number disks in interacting binaries are not an important source of angular momentum transport, they still persist in the outer parts of the disk, where the tidal effects of the binary companion are largest. One can thus envisage an analogous situation in a supermassive binary black hole in an AGN: the tidal effects of the companion can excite spiral waves in the outer parts of the accretion disk around the primary, which is the expected formation site of double-peaked emission lines.

In its simplest form, the collimated outflow model can make testable predictions. If one assumes that emission from the two oppositely directed sides of the outflow varies in concert (e.g., if the lines are excited by a central, isotropic source of ionizing radiation), then the blue peak of the resulting double-peaked line profile will be observed to respond before the red to changes in the continuum, as a result of different light-travel times. It is also possible, however, that the line emission is excited by deposition of mechanical energy by the jet onto entrained material. In such a case, local variations in the physical conditions on side of the outflow (e.g., as a result of shocks) can cause the two peaks of the line to vary independently of each other.

To summarize, the expected variability timescales are generally rather long, namely they range from a decade in the best case to a few centuries (but can be of the order of a year or less for a black hole with $M \lesssim 10^6 M_\odot$). Since many models are specific enough to make definite predictions about the evolution of the line profiles, they can be tested by comparing their predictions with observations of line profiles that span a period of only a few years. It is also noteworthy that in most models the predicted variability timescale depends ultimately on the mass of the central black hole, which is extremely uncertain, at best. It is thus quite possible that significant variability can be observed on timescales much shorter than what is estimated above.

A rare example of well-documented profile variability is that of 3C 390.3 (Veilleux & Zheng 1991; Zheng et al. 1991). Hα and Hβ spectra covering the period 1974–1988 showed the *relative* sizes of the two peaks to vary significantly over the monitoring period. In particular, the ratio of flux in the blue peak to flux in the red peak started out being greater than 1, then gradually decreased below 1, and then returned to being greater than 1. The duration of this sequence of variations was about 10 yr. A gradual change in the velocity of the blue peak was also found. A precessing elliptical disk *cannot* account for the observed variations in this object because the observed variability timescale was very short. In a luminous AGN like 3C 390.3 one expects the black hole mass to be of order $10^8 M_\odot$, for which equation (24) predicts a disk precession period of several

hundred to a thousand years. Models of inhomogeneous disks, such as disks with bright spots (Veilleux & Zheng 1991; Zheng et al. 1991) or disks with spiral waves (Chakrabarti & Wiita 1994) are quite promising in this particular case because they can explain both the variability timescale and the observed profile variations. Collimated outflow models are also capable of explaining the observations.

5. SUMMARY AND CONCLUSIONS

We have computed the expected profiles of emission lines originating in a relativistic eccentric disk. Our calculation follows the spirit of CHF and CH and is motivated by observations of double-peaked emission lines in AGNs which show that in some fraction of the cases the line profiles are asymmetric in the opposite sense than what homogeneous, relativistic, circular disk models would predict. Using the elliptical disk model we were able to fit a large fraction of the observed double-peaked profiles from the collection of EH which cannot be reproduced by circular disk models, and in addition also the Hα profile of NGC 1097. We have suggested two possible scenarios for the formation of eccentric accretion disks in AGNs: in the first scenario, the disk around a supermassive black hole can become eccentric due to the tidal effects of a secondary black hole (of mass several times smaller than that of the primary), while in the second scenario the disk is eccentric because it forms from the debris released by the tidal disruption of a star by a supermassive black hole.

Because there are several alternative models for the origin of asymmetric, double-peaked emission lines in AGNs, it is very difficult at present (and perhaps impossible) to distinguish among them using the observed line profiles alone. Rather, it is necessary to look for profile variability which may provide the key to ruling out some of the competing models. To this end we have estimated the timescale for profile variability due to precession of the elliptical disk in our two proposed scenarios and we have presented a sequence of model profiles which show how the profiles are expected to evolve as the disk pre-

cesses. For comparison we also summarize briefly and discuss the predictions of other models for double-peaked emission lines.

The variability timescales predicted by most of the models summarized in the previous section are usually very long (of the order of decades or centuries) and hence do not permit one to carry out sensitive tests based only on this timescale. Moreover, the timescales depend critically on the mass of the central black hole which is, in practice, unknown. In order to use observations of profile variability to discriminate among models of the origin of the emission lines it is necessary to compare the observed *evolution* of the profile with detailed model predictions. Hence, there is a great need for observations of the behavior of candidate objects over several years, or even decades. Attempts in this direction have already been made by Veilleux & Zheng (1991) and Zheng et al. (1991) who have concentrated on 3C 390.3, and by Halpern & Filippenko (1988, 1992) who have focused on Arp 102B. Double-peaked emission lines and their variability provide the most direct clues about the kinematics of the line-emitting gas, and thus understanding their origin can hardly be overestimated. It is therefore worthwhile to continue to monitor the unusual line profiles of the (currently) small class of double-peaked emitters, in the hope that they will display extreme examples of behavior that is not easily recognized among the ordinary majority of AGNs, and provide us with clues for the origin of their emission lines.

REFERENCES

Bardeen, J. M., & Peterson, Y. A. 1975, ApJ, 195, L65
Begelman, M. C., Blandford, R. D., & Rees, M. J. 1980, Nature, 287, 307
Bunk, W., Livio, M., & Verbunt, F. 1990, A&A, 232, 371
Busko, I. C., & Steiner, J. E. 1990, MNRAS, 245, 470
Cannizzo, J. K., Lee, H. M., & Goodman, J. 1990, ApJ, 351, 38
Chakrabarti, S., & Wiita, P. J. 1993a, A&A, 271, 216
———. 1993b, ApJ, 411, 602
———. 1994, ApJ, submitted
Chen, K., & Eardley, D. 1991, ApJ, 382, 125
Chen, K., & Halpern, J. P. 1989, ApJ, 344, 115 (CH)
Chen, K., Halpern, J. P., & Filippenko, A. V. 1989, ApJ, 339, 742 (CHF)
Dumont, A. M., & Collin-Souffrin, S. 1990, A&A, 229, 313
Eracleous, M., & Halpern, J. P. 1994, ApJS, 90, 1 (EH)
Evans, C. R., & Kochanek, C. S. 1989, ApJ, 346, L13
Fabian, A. C., Rees, M. J., Stella, L., & White, L. 1989, MNRAS, 238, 729
Frank, J., King, A. R., & Raine, D. J. 1992, Accretion Power in Astrophysics (Cambridge: Cambridge Univ. Press)
Gaskell, C. M. 1983, in Quasars and Gravitational Lenses, Proc. 24th Liège Astrophysical Colloq. (Liège: Institut d'Astrophysique, Univ. Liège), 473
Halpern, J. P. 1990, ApJ, 365, L51
Halpern, J. P., & Filippenko, A. V. 1988, Nature 331, 46
———. 1992, in AIP Conf. Proc. No. 254, Testing the AGN Paradigm, ed. S. S. Holt, S. G. Neff, & C. M. Urry (New York: AIP), 57
Hirose, M., & Osaki, Y. 1990, PASJ, 42, 135
———. 1992, PASJ, 45, 595
Horne, K., & Marsh, T. R. 1986, MNRAS, 218, 761
Horne, K., & Saar, S. H. 1991, ApJ, 374, L55

Kim, S.-W., & Yee, I. 1992, in AIP Conf. Proc. No. 254, Testing the AGN Paradigm, ed. S. S. Holt, S. G. Neff, & C. M. Urry (New York: AIP), 239
Kinney, A. L. 1992, in AIP Conf. Proc. No. 254, Testing the AGN Paradigm, ed. S. S. Holt, S. G. Neff, & C. M. Urry (New York: AIP), 139
———. 1994 in The First Stromlo Symposium: The Physics of Active Galaxies, ed. G. V. Bicknell, M. A. Dopita, & P. J. Quinn (San Francisco: ASP), 61
Kochanek, C. S. 1994, ApJ, 422, 508
Livio, M. 1992, in Interacting Binaries ed. H. Nussbaumer, & A. Orr (Berlin: Springer), 135
Lubow, S. 1991a, ApJ, 381, 259
———. 1991b, ApJ, 381, 268
———. 1992, ApJ, 401, 317
Netzer, H. 1992, in AIP Conf. Proc. No. 254, Testing the AGN Paradigm, ed. S. S. Holt, S. G. Neff, & C. M. Urry (New York: AIP), 146
Norman, C., & Miley, G. 1984, A&A, 141, 85
Oke, J. B. 1987, in Superluminal Radio Sources, ed. J. A. Zensus & T. J. Pearson (Cambridge: Cambridge Univ. Press), 267
Osaki, Y. 1989, PASJ, 41, 1005
Patterson, J., Haplern, J. P., & Shambrook, A. 1993, ApJ, 419, 803
Pérez, E., Penston, M. V., Tadhunter, C., Mediavilla, E., & Moles, M. 1988, MNRAS, 230, 356
Phillips, M. M., Pagel, B. E. J., Edmunds, M. G., & Díaz, A. 1984, MNRAS, 210, 701
Press, W. H., & Teukolsky, S. A. 1977, ApJ, 213, 183
Rees, M. J. 1988, Nature, 333, 523
———. 1990, Science, 247, 817
Roos, N. 1992, ApJ, 385, 108

Savonije, G. J., Papaloizou, J. C. B., & Lin, D. N. C. 1994, MNRAS, 268, 13
Shakura, N. I., & Sunyaev, R. A. 1973, A&A, 24, 337
Sparks, W. B., Biretta, J. A., & Machetto, F. 1994, ApJS, 90, 909
Storchi-Bergmann, T., Baldwin, J. A., & Wilson, A. S. 1993, ApJ, 410, L11 (SBW)
Syer, D., & Clarke, C. J. 1992, MNRAS, 255, 92
———. 1993, MNRAS, 260, 463
Syer, D., Clarke, C. J., & Rees, M. J. 1991, MNRAS, 250, 505
Veilleux, S., & Zheng, W. 1991, ApJ, 377, 89
Vogt, N. 1982, ApJ, 252, 653

Warner, B. 1985, in Interacting Binaries, ed. P. P. Eggleton & J. E. Pringle (Dordrecht: Reidel), 367
Weinberg, S. 1972, Gravitation and Cosmology (New York: Wiley), 197
Whitehurst, R. 1988, MNRAS, 232, 35
———. 1994, MNRAS, 266, 35
Wilson, A. S. 1993, in Astrophysical Jets, eds. D. Burgarella, M. Livio, & C. P. O'Dea (Cambridge: Cambridge Univ. Press), 121
Zheng, W., Binette, L., & Sulentic, J. W. 1990, ApJ, 365, 115
Zheng, W., Veilleux, S., & Grandi, S. A. 1991, ApJ, 381, 418